Electronic Supplementary Material (ESI) for Journal of Materials Chemistry A.
This journal is © The Royal Society of Chemistry 2015

Supporting Information

Hierarchical assembly and superior sodium storage properties of sea-sponge structural C/SnS@C nanocomposite

Shipei Chen,[‡a] Ke Xing,[‡a] Jiahao Wen,[b] Ming Wen,*[a] Qingsheng Wu [a] and Yi Cui [c]

[a] School of Chemical Science and Engineering, Shanghai Key Laboratory of Chemical Assessment and Sustainability, Tongji University, Shanghai 200092, China.

[b] School of Electrical Engineering, Chongqing University, Chongqing 400044, China.

[c] Department of Materials Science and Engineering, Stanford University, Stanford, California 94305, USA.

Corresponding author.

E-mail: m_wen@tongji.edu.cn (M. Wen)

‡ These authors contributed equally to this work.

Materials and Methods:

Chemicals. Tin(IV) chloride ($SnCl_4 \cdot 5H_2O$, ≥99.8%), thioacetamide (CH_3CSNH_2, ≥98%), ethylene glycol ($C_2H_6O_2$, ≥99.0%), ethanol (C_2H_6O, ≥99.7%), sodium chloroacetate ($ClCH_2COONa$, ≥98%), glucose ($C_6H_{12}O_6$, ≥99.8%), sodium (Na, ≥99%)were purchased from Sinopharm Chemical Reagent Co., Ltd. Electrolyte (1M NaClO4 in EC/PC 1:1 by volume with FEC 5wt%) was purchased from Shanghai Xiaoyuan Energy Technology Co. Ltd. All the reagents were analytical purity and used without further purification.

Synthesis of S-MCSs. The S-MCSs are prepared by ultrasonically nebulizing aqueous solutions of sodium chloroacetate ($ClCH_2COONa$, 1.5 M) into droplets using a household humidifier, an Ar flow carries the droplets into a furnace with 700℃, after precursor decomposed, the product is collected in water bubblers with the generated salt dissolving, leaving behind the S-MCSs. Subsequently, the products were centrifuged and washed with ethanol and water, and dried overnight in a vacuum oven at 80 °C.

Supporting Figures for Discussion

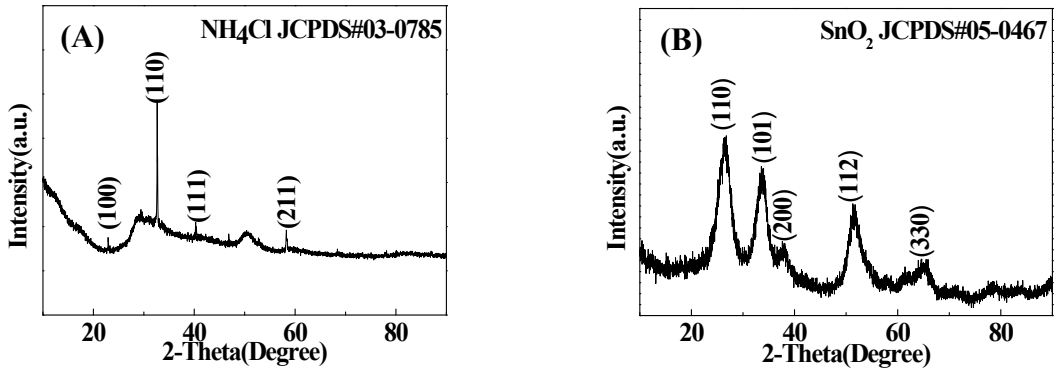

Fig. S1 XRD patterns: (A) Products obtained in ethanol solvent without deionized water washing; (B) Products synthesized in water solvent.

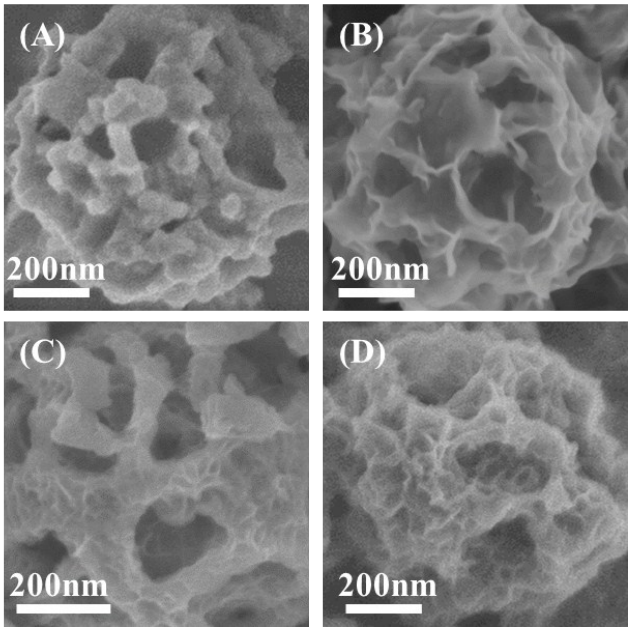

Fig. S2 SEM images of C/SnS_2 composite obtained at 25℃ in ethanol solvent within different reaction time: 6 hrs (A), 12 hrs (B), 24 hrs (C), and 48 hrs(D).

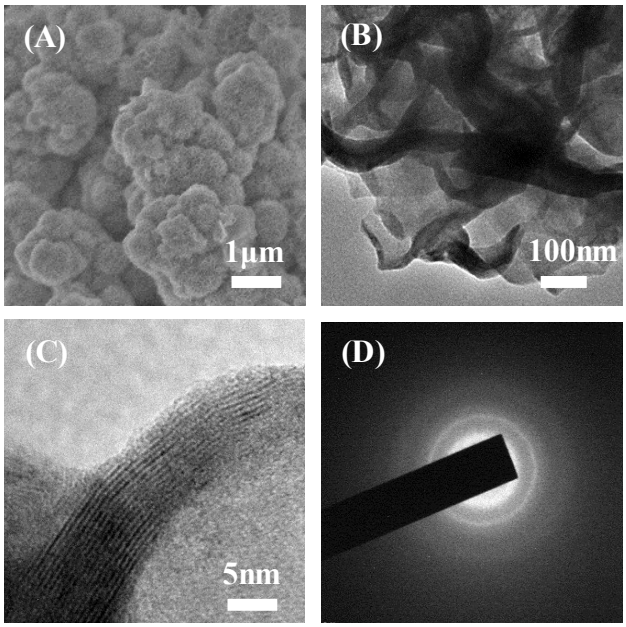

Fig. S3 SnS_2 prepared without S-MCSs engaging: (A) SEM image; (B) TEM iamge; (C) HRTEM image; (D) SAED pattern.

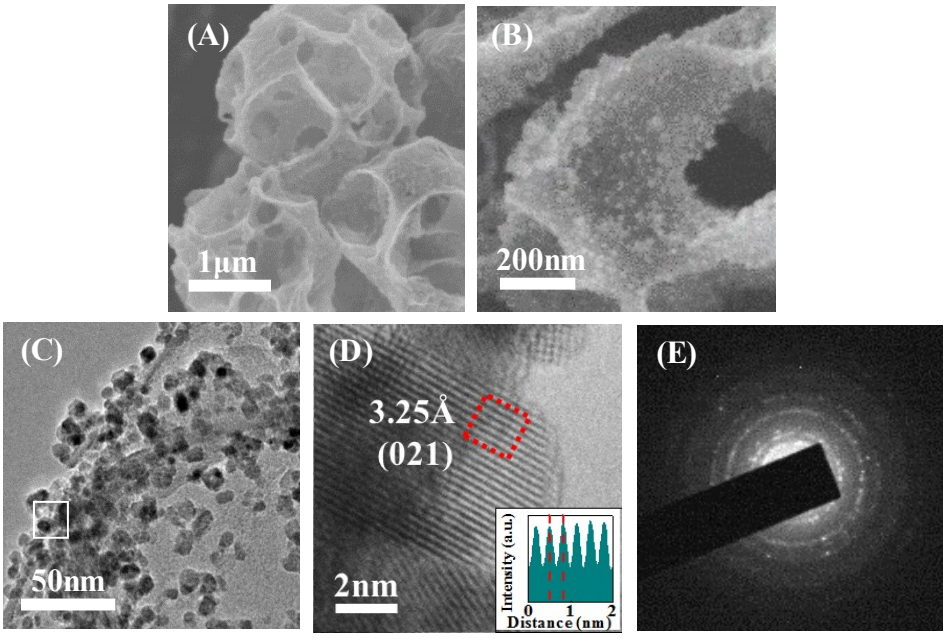

Fig. S4 C/SnS nanocomposite prepared under argon by heating treatment of C/SnS_2 at 500°C for 3 hrs: (A,B) SEM image; (C) TEM image; (D) HETEM image from marked area in (C); (E) SAED pattern of SnS NPs on S-MCSs.

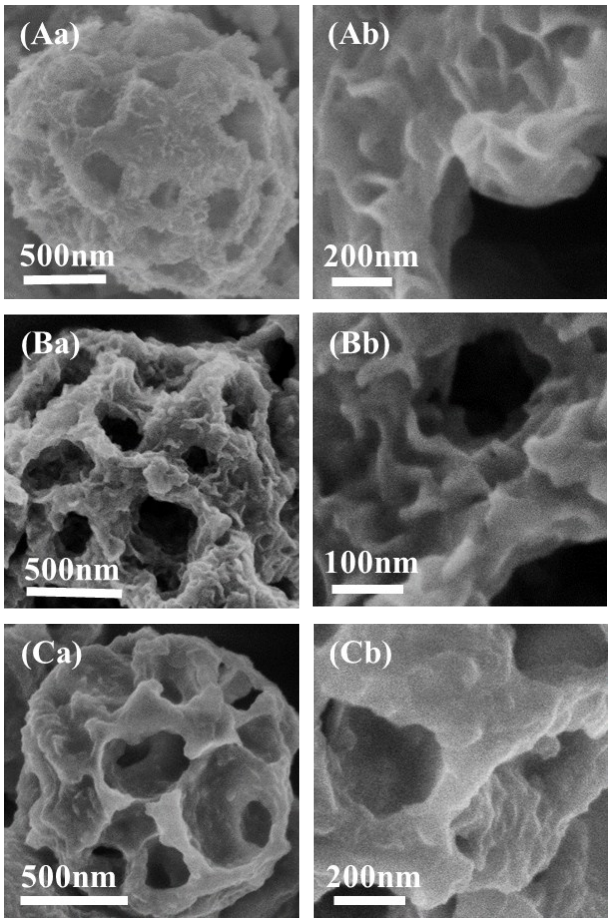

Fig. S5 SEM images in low (a) and high (b) magnification of C/SnS_2@pGlu prepared at hydrothermal time of 6 hrs (A), 12 hrs (B) and 24 hrs (C).

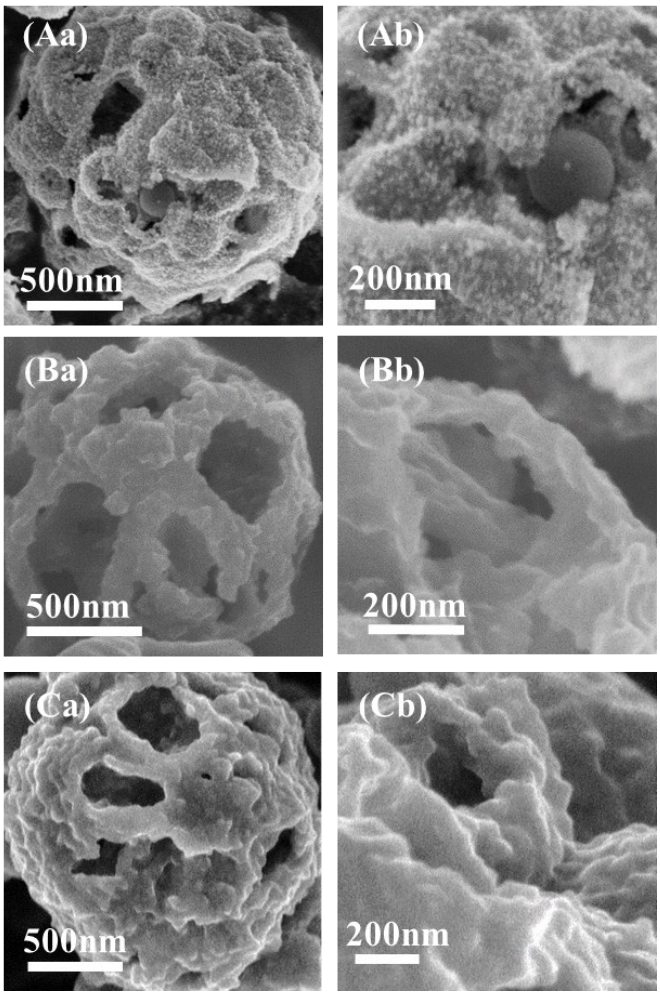

Fig. S6 SEM images in low (a) and high (b) magnification of C/SnS_2@pGlu prepared at glucose concentration at 0.75 M (A), 1.0 M (B) and 1.25 M (C).

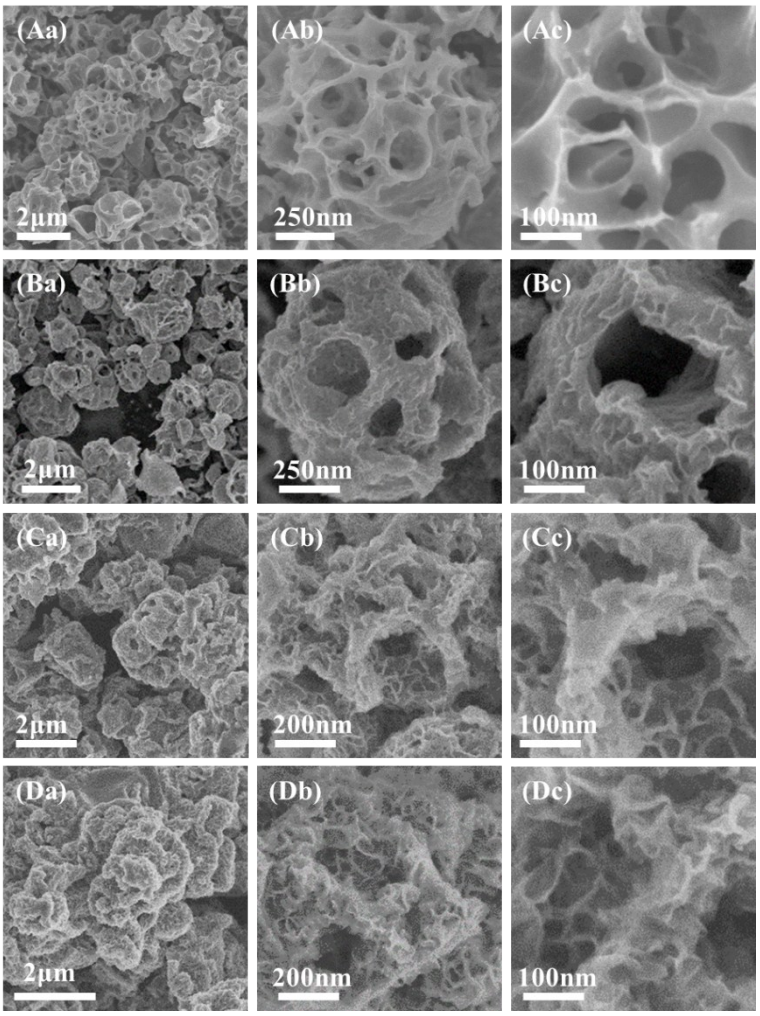

Fig. S7 SEM images in different magnification of C/SnS_2 prepared at Sn^{4+}concentration at 5 mM (A), 10 mM (B), 15 mM (C) and 20 mM (D), respectively.

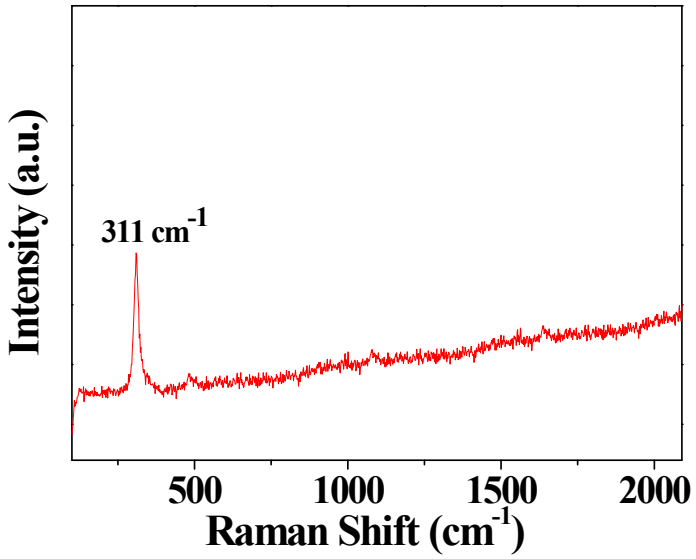

Fig. S8 Raman spectra of SnS_2 nanoflakes in the wavelength range of 100–2100 cm^{-1}.

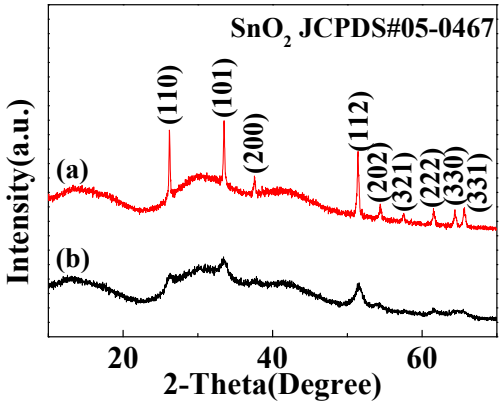

Fig. S9 XRD patterns of TG measured residue substances of SnO2 for C/SnS_2 (a) and C/SnS@C (b).

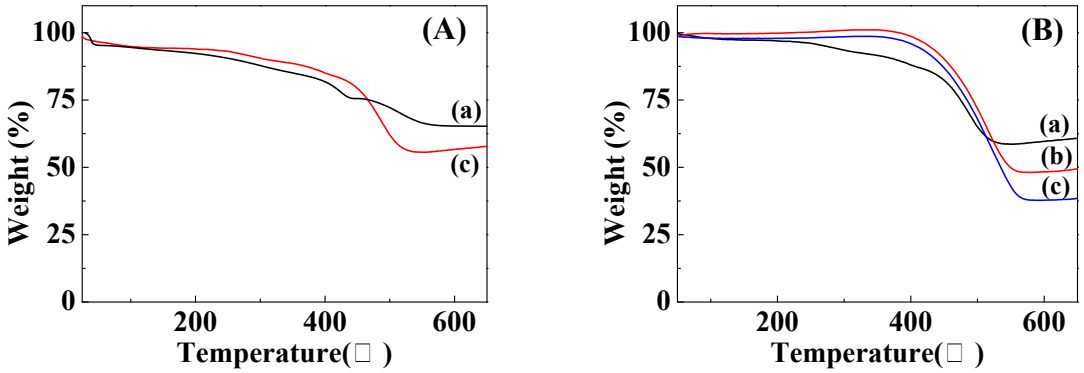

Fig. S10 TG curves under Air of C/SnS_2 (A) and C/SnS@C (B) prepared in different concentration of Sn4+ at 20 mM (a), 15 mM (b), and 10 mM(c).

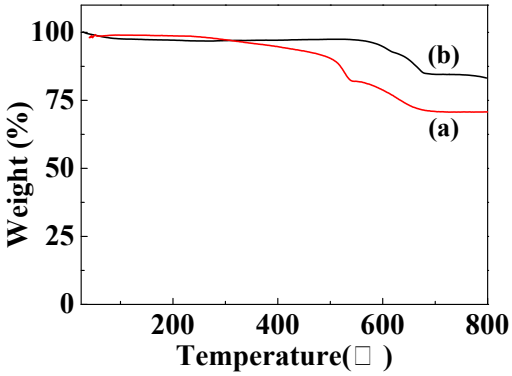

Fig. S11 TG curves under N_2 of C/SnS_2@pGlu (a) and pure SnS_2 (b).

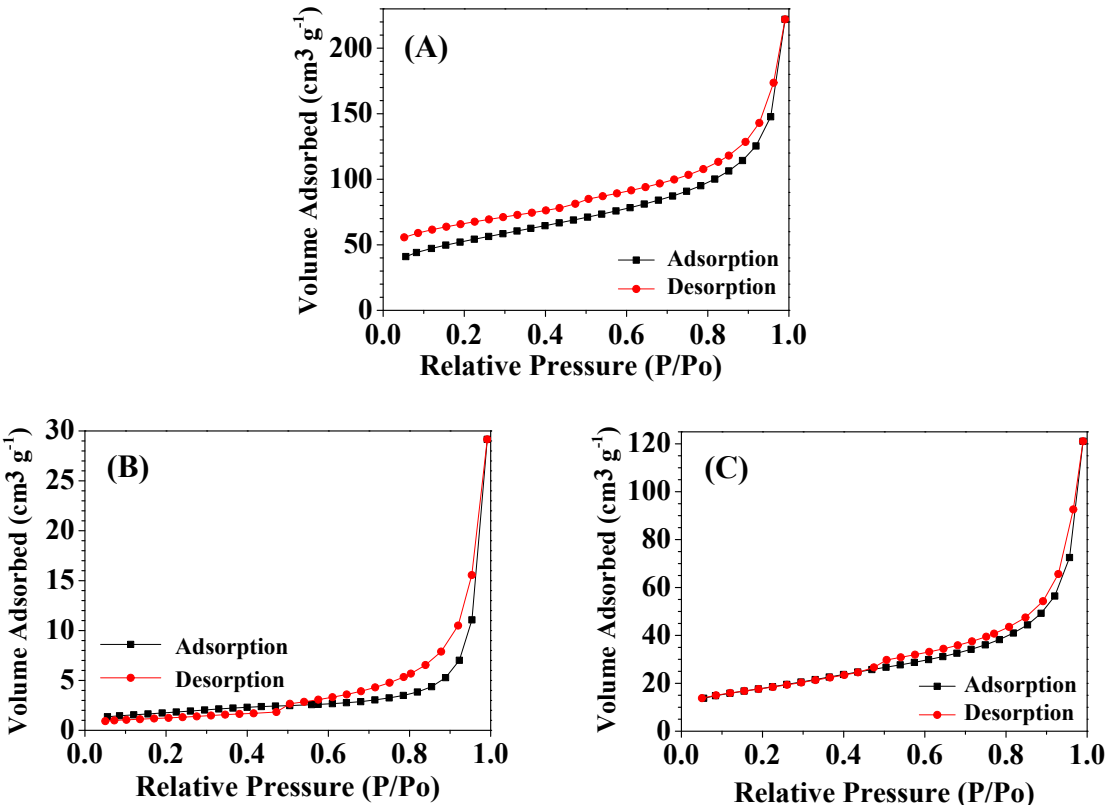

Fig. S12 N_2 adsorption-desorption isotherms of S-MCSs (A), SnS_2 (B) and C/SnS_2 (C).

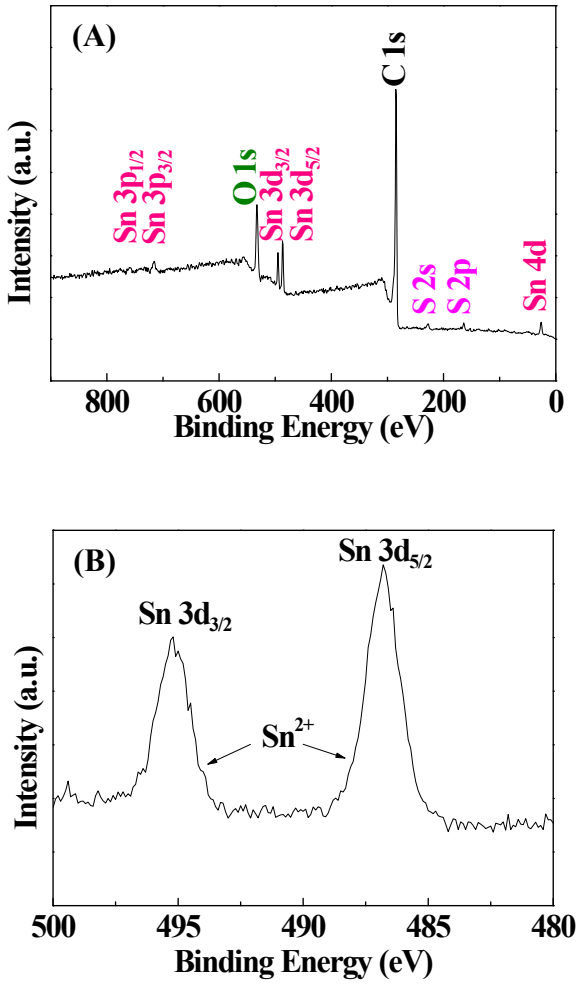

Fig. S13 XPS full spectra (A) and Sn 3d (B) of C/SnS.

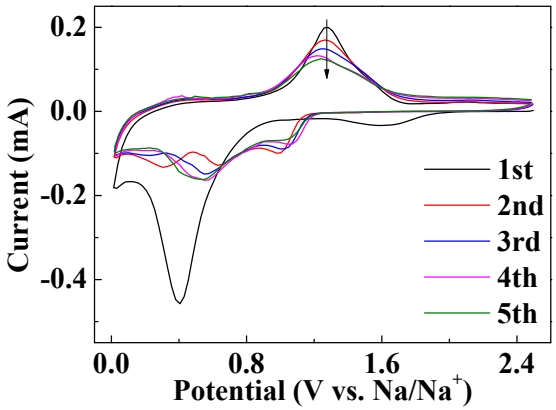

Fig. S14 CV curves of C/SnS_2 for the first 5 cycles at 0.1 mV s^{-1}.

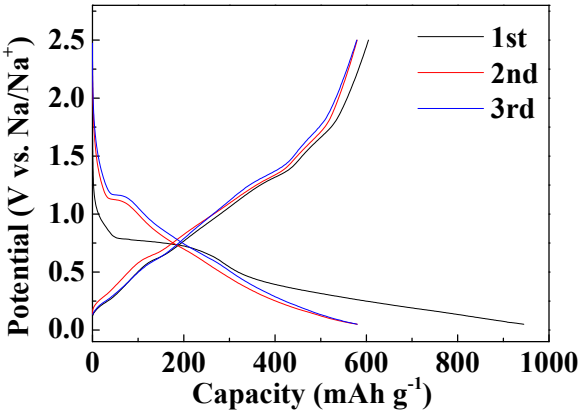

Fig. S15 Galvanostatic charge-discharge profiles for C/SnS@C at 0.1 A g^{-1} for the first three cycles.

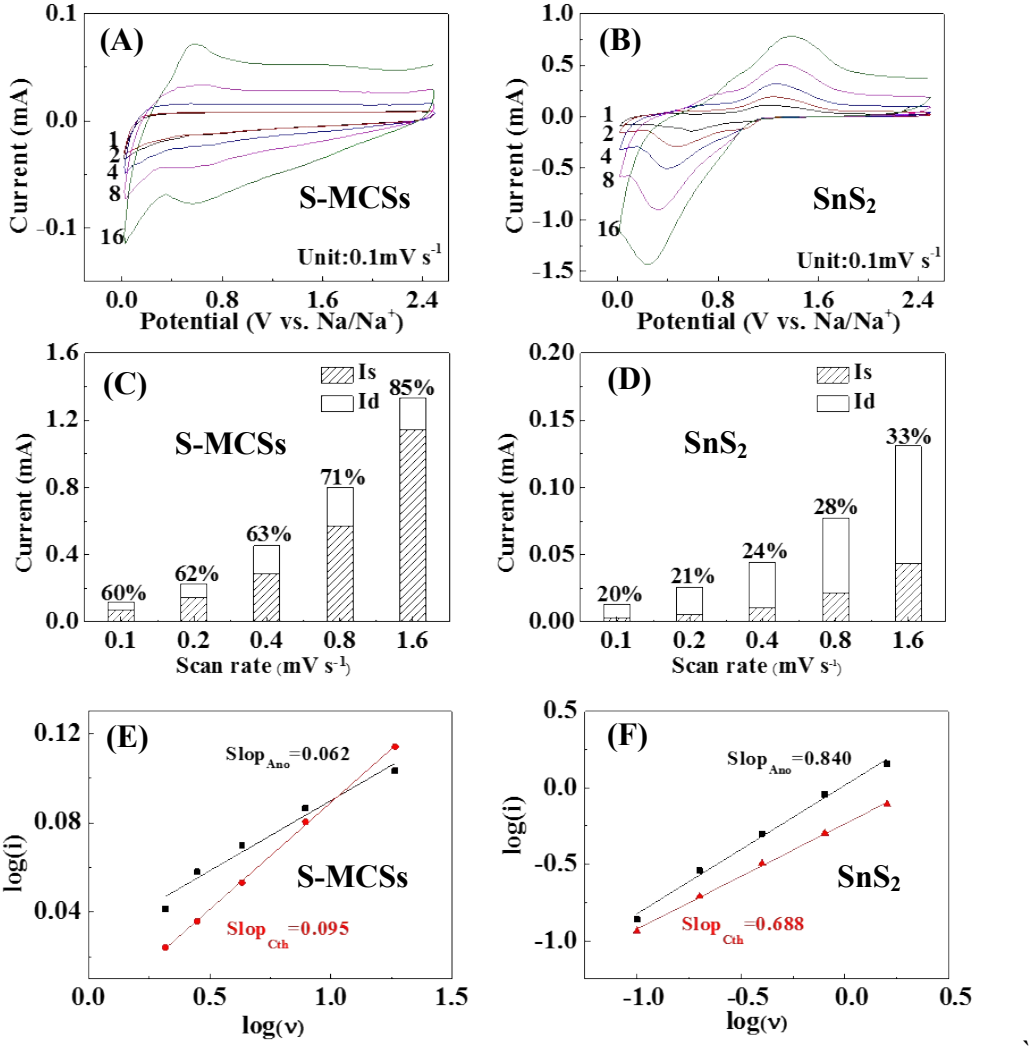

Fig. S16 (A,B) CV curves of S-MCSs and SnS_2 at scan rate from 0.1 to 1.6 mV s^{-1}; (C, D) Capacity separation diffusion-controlled Id and capacitive Is for anodic peak in S-MCSs and SnS_2; (E, F) Relationships for S-MCSs and SnS_2 between the log i (peak current) and log v (scan rate) in anodic process and cathodic process (scanning rate between 0.1-1.6 mV s^{-1}).

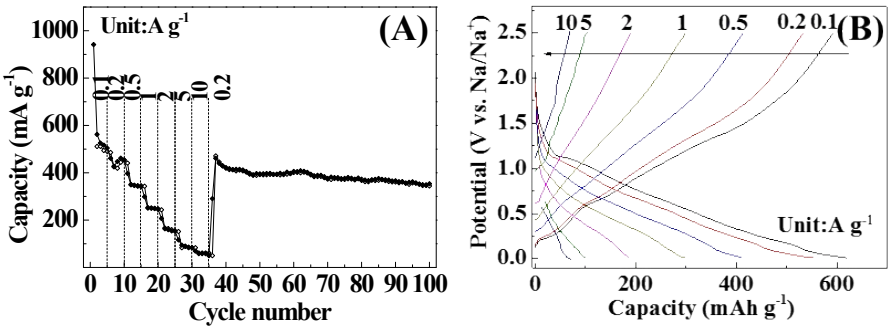

Fig. S17 Rate performance of C/SnS (A); Galvanostatic charge-discharge profiles for C/SnS in the potential range of 0.01-2.5 V (vs. Na/Na+) at different current density (B).

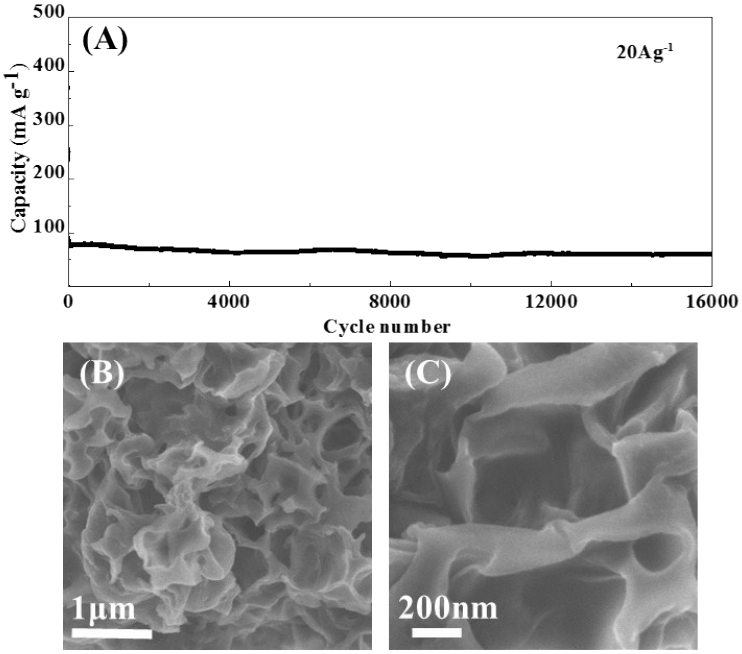

Fig. S18 (A) Cycling performance of S-MCSs at 20 A g^{-1}; SEM images of S-MCSs in low magnification (B) and high magnification (C) after 16000 cycles.

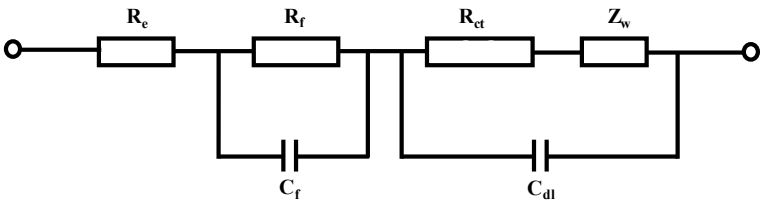

Fig. S19 Randle-type equivalent circuit model for S-MCSs, SnS_2, C/SnS_2, C/SnS, and C/SnS@C electrodes. R_e: the electrolyte resistance; C_f and R_f: the capacitance and resistance of the SEI film and contact corresponding to the high-frequency semicircle, respectively; C_{dl} and R_{ct}: the double-layer capacitance and charge transfer resistance related to the middle-frequency semicircle, respectively; Z_w: the Warburg impedance related to the diffusion of Na-ion into the bulk of composite electrodes.

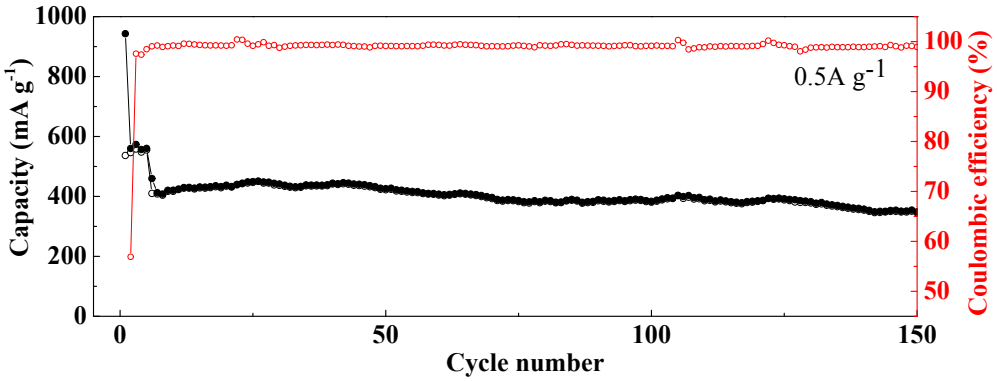

Fig. S20 Cycling performance of C/SnS@C at a current density of 0.5 A g^{-1}

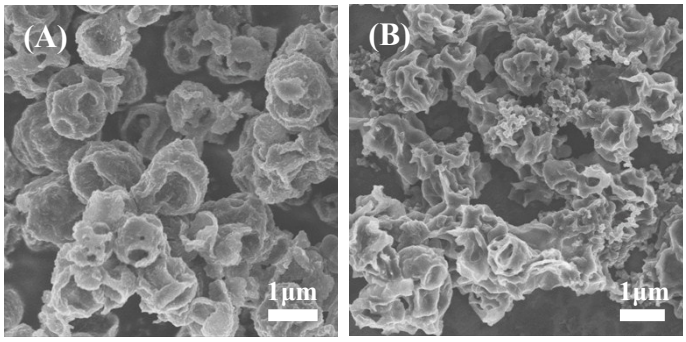

Fig. S21 The low-resolution SEM images of C/SnS@C for fresh (A) and after 300 cycles (B).

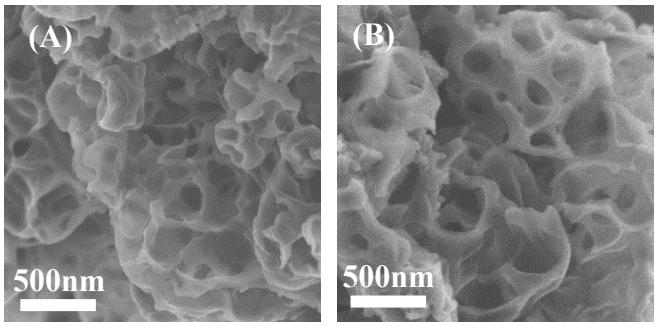

Fig. S22 SEM images of C/SnS_2 (A) and C/SnS (B) electrode after 300 cycles.

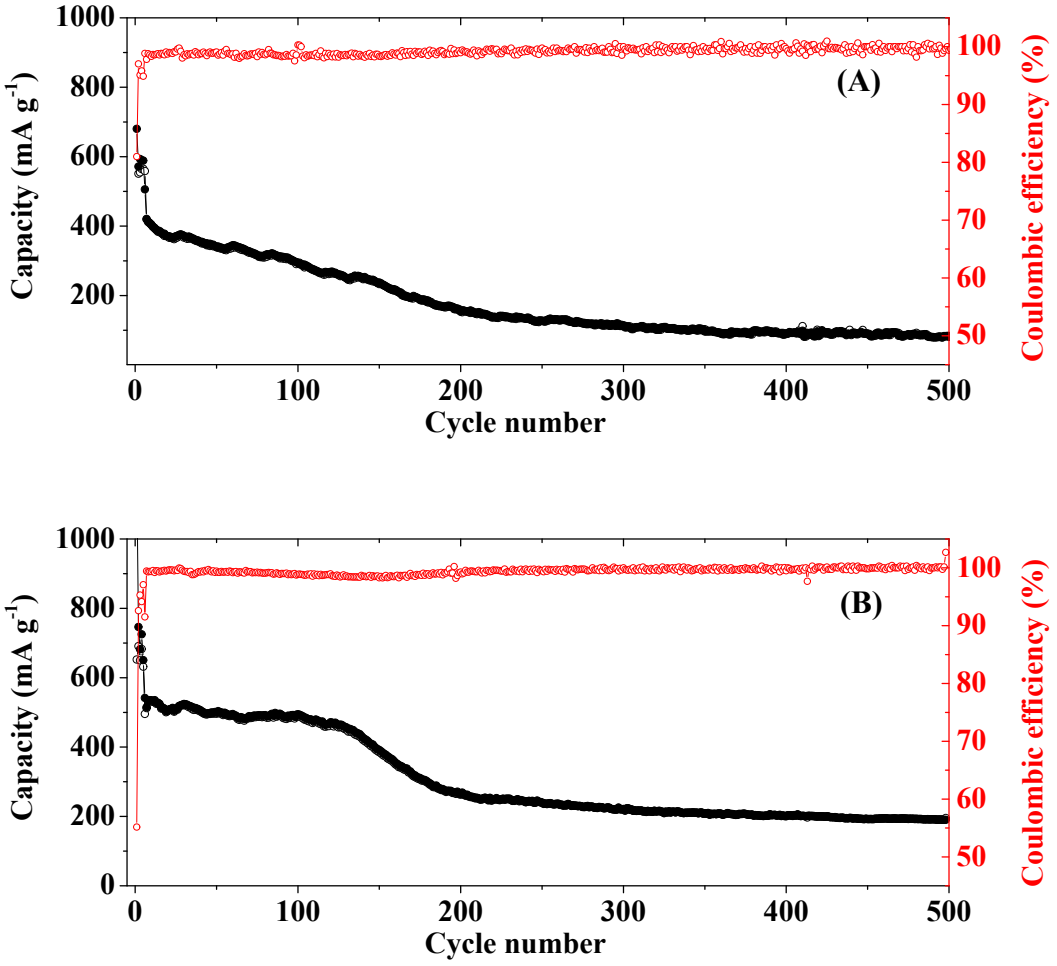

Fig. S23 Cyclic performances of C/SnS_2 (A) and C/SnS (B) at 1 A g^{-1}.

Tab. S1 Rate performance compare with other reported works in literatures.

Materials		C/SnS@C	MoS_2/CNTs	$MoSe_2$/CNT	$FeSe_x$-rGO	SnS/C	SnS@RGO
Current density ($A\ g^{-1}$)	0.1	550	–	–	–	419	405
	0.2	530	450	382	478	–	351
	0.5	430	320	346	423	334	–
	1	350	–	–	377	310	–
	2	280	–	–	342	–	–
	5	190	–	255	250	205	–
Ref.(year)		this work	41(2014)	42(2016)	43(2016)	25(2015)	18(2015)

Tab. S2 Kinetic parameters of S-MCSs, SnS_2, C/SnS_2, C/SnS, and C/SnS@C electrodes after 5 cycles.

Samples	R_{ct} [Ω]	R_{ct} fit accuracy
S-MCSs	211	4.7%
SnS_2	1016	3.2%
C/SnS_2	630	2.5%
C/SnS	695	2.2%
C/SnS@C	259	2.0%

Tab. S3 Simulation results of the EIS spectra using the Randle-type equivalent circuit equivalent circuit shown in Fig. 5D.

Cycle	R_f [Ω]	R_f fit accuracy	R_{ct} [Ω]	R_{ct} fit accuracy
Fresh	–	–	1324	3.6%
1^{st}	18	6.1%	82	5.1%
300^{th}	3.7	5.2%	194	1.7%